

CLOAK: Contrastive Guidance for Latent Diffusion-Based Data Obfuscation

Xin Yang
University of Alberta
 Edmonton, AB, Canada
 xin.yang@ualberta.ca

Omid Ardakanian
University of Alberta
 Edmonton, AB, Canada
 oardakan@ualberta.ca

Abstract—Data obfuscation is a promising technique for mitigating attribute inference attacks by semi-trusted parties with access to time-series data emitted by sensors. Recent advances leverage conditional generative models together with adversarial training or mutual information-based regularization to balance data privacy and utility. However, these methods often require modifying the downstream task, struggle to achieve a satisfactory privacy-utility trade-off, or are computationally intensive, making them impractical for deployment on resource-constrained mobile IoT devices. We propose CLOAK, a novel data obfuscation framework based on latent diffusion models. In contrast to prior work, we employ contrastive learning to extract disentangled representations, which guide the latent diffusion process to retain useful information while concealing private information. This approach enables users with diverse privacy needs to navigate the privacy-utility trade-off with minimal retraining. Extensive experiments on four public time-series datasets, spanning multiple sensing modalities, and a dataset of facial images demonstrate that CLOAK consistently outperforms state-of-the-art obfuscation techniques and is well-suited for deployment in resource-constrained settings.

I. INTRODUCTION

Ubiquitous and personal sensing through the Internet of Things (IoT), mobile and wearable devices, has driven significant advances in mobile health, home automation, and other domains where the continuous collection of sensor data is essential. For example, smartwatches equipped with Inertial Measurement Units (IMUs) capture multivariate time-series data that may be transmitted to the cloud, where powerful machine learning models infer useful, non-private attributes, such as the user’s physical activity. However, sharing raw sensor data with semi-trusted third parties raises serious privacy concerns. This is because although these parties are trusted to faithfully perform desired inferences on the data, they may also carry out unwanted inferences to extract and monetize *private attributes* embedded in this data, without the user’s knowledge or consent. For instance, motion data collected for fitness tracking could inadvertently reveal sensitive demographic traits or health conditions [1]. These *attribute inference attacks* threaten user privacy and pose a barrier to the broader adoption of ubiquitous and personal sensing technologies.

Protecting private attributes in time-series data emitted by sensors presents unique challenges that render many privacy-preserving techniques inadequate. First, this type of data may contain information about private and non-private (i.e.

public) attributes that are not directly recorded by the sensors (e.g. motion data captured by an IMU usually contains some information about an individual’s age or health condition). While such latent attributes can be uncovered through deep learning, they cannot be easily redacted or perturbed because they are not explicitly represented in the raw data. This problem is compounded by the fact that in a lower-dimensional space, features relevant to private and public attributes often overlap—a phenomenon known as *entanglement*. Thus, redacting or perturbing these features to protect privacy can severely degrade data utility, leading to an inevitable trade-off between utility and privacy. Second, Differential Privacy (DP), which is widely regarded as a gold standard for verifiable privacy, has limited applicability in this setting. Traditional DP mechanisms are primarily designed to defend against membership inference attacks, rather than attribute inference attacks that exploit data reported by a specific user to infer their private attributes. Even in the local setting, DP mechanisms are not designed to prevent inference of latent private attributes, i.e. private attributes that are not directly represented in an individual’s reported data. Moreover, applying DP noise to features that correlate with private attributes requires learning a fully disentangled representation—an objective that has proven difficult to achieve in practice [2]. Third, techniques based on cryptographic primitives, such as secure multi-party computation or homomorphic encryption [3], are too computationally intensive for deployment on resource-constrained devices.

Generative models, particularly Generative Adversarial Networks (GANs), ushered in a new paradigm of data obfuscation. GAN-based obfuscation techniques suppress information about private attributes and preserve information relevant to public attributes in the data [1], [4]. The obfuscated data remains in the same space as the raw sensor data, allowing it to be seamlessly used by downstream applications. However, GAN-based obfuscation methods suffer from well-known problems. The adversarial min-max game between the generator and discriminator is notoriously unstable and difficult to train. More critically, the definition of private attributes shapes the discriminator’s objective, which in turn influences the generator during training. Consequently, any change in the private attribute definition or the user’s preferred privacy-utility trade-off requires costly retraining of the entire model. These issues make GAN-based approaches poorly

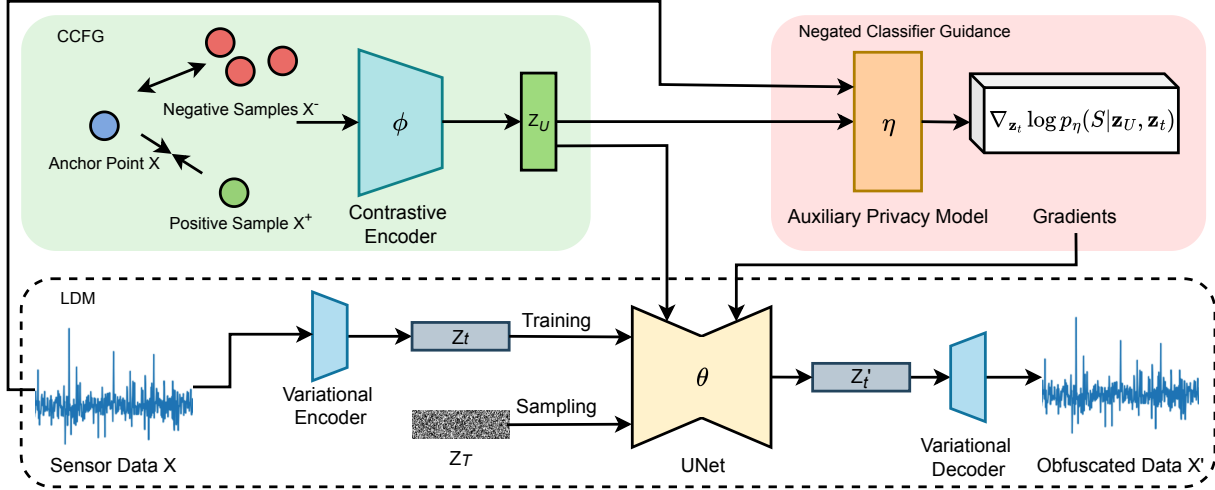


Fig. 1. Overview of CLOAK’s architecture.

suited for accommodating diverse privacy needs or adapting to individual user preferences. Recent work by Yang *et al.* [5] introduced PrivDiffuser, a diffusion model-based obfuscation framework that achieves a strong privacy-utility trade-off, outperforming GAN-based models. However, its obfuscation process is computationally intensive, making it less suitable for deployment on resource-constrained devices. Moreover, PrivDiffuser relies on regularization based on the estimated mutual information to learn disentangled representations of public and private attributes, which is only partially successful in practice.

We propose a novel sensor data obfuscation framework that leverages the power of diffusion models while addressing the limitations of prior work. CLOAK utilizes a latent diffusion model to perform data obfuscation in a lower-dimensional space, and a variational autoencoder (VAE) to map between the latent and original input spaces. This significantly reduces the computational overhead typically associated with diffusion models, making CLOAK well-suited for deployment on mobile IoT platforms. We introduce a novel conditioning method, named Contrastive Classifier-Free Guidance (CCFG), to guide the latent diffusion process with disentangled public attribute representations, achieving a superior privacy-utility trade-off. Additionally, we incorporate Negated Classifier Guidance to condition the diffusion model on private attributes, enabling effective removal of information about these attributes at sampling time. Together, these guidance techniques allow CLOAK to support diverse user privacy preferences with minimal retraining effort (see Figure 1). Our contributions are summarized below:

- We propose CLOAK, a novel and lightweight obfuscation framework that leverages latent diffusion to mitigate attribute inference attacks on sensor-generated time-series.
- We introduce two novel guidance techniques for CLOAK: Contrastive Classifier-Free Guidance to preserve information about the public attribute(s) and Negated Classifier Guidance to suppress information about the private attribute(s), together enabling fine-grained control over the privacy-utility trade-off.

tion about the public attribute(s) and Negated Classifier Guidance to suppress information about the private attribute(s), together enabling fine-grained control over the privacy-utility trade-off.

- We conduct extensive experiments on five datasets covering multiple sensing modalities. CLOAK consistently outperforms state-of-the-art generative obfuscation methods on sensor-emitted time-series and images.

II. RELATED WORK

A. Anonymization and Obfuscation of Sensor Data

Privacy protection in sensor data can be achieved by learning a low-dimensional representation that contains no information about the private attribute(s) ideally, then sending only this representation to the service provider. Early work in this area, such as Privacy Adversarial Network (PAN) [6] and DeepObfuscator [7], focuses on training an encoder for feature extraction in an adversarial fashion, ensuring that a discriminator cannot recognize the private attribute from the learned representation. TIPRDC [8] uses mutual information-based regularization instead to minimize the privacy loss. Since the representations learned by these approaches are not in the original input space, downstream applications must be modified to consume this data, posing a non-trivial challenge for real-world deployment.

To overcome this challenge, conditional generative models have been utilized to generate privacy-preserving synthetic data that has the same dimension as the raw sensor data. For example, GANs have been used for editing images and videos to protect sensitive information [11], [12], [13]; however, these methods are not directly applicable to obfuscate time-series as they are specifically designed for visual data based on the higher-dimensional structure. To obfuscate sensor-generated time-series, Malekzadeh *et al.* [1] proposed training an autoencoder by adding multiple regularization terms to

TABLE I
COMPARISON BETWEEN CLOAK AND PRIOR WORK ON PRIVACY PROTECTION FOR SENSOR DATA.

	Requires no changes to apps	Easy to accommodate diff. privacy needs	Lightweight inference
Privacy-preserving feature extraction [6], [7], [8]	✗	✗	✓
GAN-based obfuscation [1], [4], [9], [10]	✓	✗	✓
Diffusion-based obfuscation w/ MI regularization [5]	✓	✓	✗
CLOAK (LDM-based obfuscation w/ CCFG)	✓	✓	✓

its loss function to reduce privacy loss. Olympus [9] and ObscureNet [4] both used a GAN architecture, training an autoencoder-based obfuscation model, where the autoencoder aims to reconstruct sensor data so as to maintain data utility, and the discriminator acts as an attacker that tries to extract sensitive information from the reconstructed data. MaSS [10] transforms sensor data to suppress multiple private attributes for both visual and time-series sensor data by combining information-theoretic measures with adversarial training. Yet, MaSS requires fine-tuning the models used in downstream applications, which cannot be done when the service provider is unaware of whether users have obfuscated their data. Overall, all these obfuscation models leverage GAN to obscure private attributes embedded in sensor data. However, they lack the flexibility to adapt to the diverse privacy needs of different users, because the training of the discriminator determines the definition of the private attribute, and the weight of the discriminator loss governs the privacy-utility trade-off, both of which are tightly coupled with the training of the generator. Hence, modifying the private attribute requires retraining the entire obfuscation model.

Recently, Yang and Ardakanian [5] introduced PrivDiffuser, a diffusion-based obfuscation model that achieves a better privacy-utility trade-off than GAN-based obfuscation models. To guide the diffusion process, it uses disentangled representations obtained by minimizing mutual information between public and private attribute representations. However, as we show later in the paper, this method is less effective at achieving disentanglement compared to CLOAK’s CCFG. Moreover, the sampling process of regular diffusion models is computationally intensive, making it difficult to deploy PrivDiffuser on resource-constrained devices. Table I presents a detailed comparison between CLOAK and prior work on sensor data obfuscation.

B. Learning Disentangled Representations for Synthetic Data Generation

A key challenge in sensor data obfuscation is striking a good balance between utility and privacy loss. This can be addressed by conditioning the generative model with disentangled representations of public and private attributes. In image editing tasks [14], [15], disentangled representation learning based on contrastive learning and InfoNCE [16] has been successfully integrated with GAN-based generative models. Wu *et al.* [17] showed that diffusion models, similar to GANs, can inherently learn disentangled latent spaces in text-to-image generation tasks. This property enables controlled image edit-

ing on a wide range of attributes without fine-tuning the entire diffusion model. Yang *et al.* [18] proposed DisDiff, which disentangles the gradient fields of a pre-trained diffusion model by minimizing the mutual information. NoiseCLR [19] used unsupervised contrastive learning to extract disentangled, interpretable image editing directions in diffusion-based text-to-image generation tasks. DEADiff [20] focused on decoupling the style and semantics using Q-formers in attention layers for image style transfer. These works explore using disentangled representation learning to factorize the latent space of a pre-trained diffusion model. Although they can be applied to edit certain attributes in images, they require powerful diffusion models pre-trained on images and semantics learned from text prompts, such as Stable Diffusion [21] and CLIP [22], which are not always available for other modalities, such as time-series sensor data. Another line of research has shown that the factorized latent space of diffusion models can facilitate disentangled representation learning [23], [24], [25]. However, they do not investigate using disentangled representations to train conditional diffusion models for privacy protection.

Armandpour *et al.* [26] found that the entanglement of the main prompt with a negative prompt could drastically decrease the quality of the synthesized image in a text-to-image application. They proposed Perp-Neg to alleviate this entanglement by projecting the main and negative prompts to orthogonal spaces. Yet, this method has shown difficulty in disentangling time-series sensor data [5]. CLOAK addresses these gaps by introducing a new contrastive classifier-free guidance approach.

III. THREAT MODEL

CLOAK aims to defend against an honest-but-curious (HBC) adversary that has access to sensor data \mathbf{x} shared by the user, intended for desired inferences on the public attribute(s) U . The adversary can perform intrusive inferences to uncover the user’s private attribute(s) S embedded in the shared data, known as attribute inference attacks. The definition of public attribute U is assumed to be time-invariant as it is tied to the desired downstream applications (e.g. step counting). The private attributes S are specified by users and may change over time. For other unspecified attributes R , we aim to offer some protection since the user may deem them private in the future. For example, in motion-based human activity recognition, \mathbf{x} represents motion sensor readings, U is the activity class to be inferred from \mathbf{x} , S represents the user-specified sensitive attribute (e.g., age) and R represents other unspecified attributes (e.g., height and weight). We assume

that the adversary neither has any metadata about the user, nor does it know if the shared data has been obfuscated, which is a practical assumption since obfuscation may be applied selectively or probabilistically. The adversary performs both desired inferences and intrusive inferences on a remote server, where the models can be trained on public datasets.

CLOAK aims to protect against attribute inference attacks by transforming raw sensor data \mathbf{x} into \mathbf{x}' on the user's device, then sharing \mathbf{x}' with the HBC service provider. The obfuscation process $f(\mathbf{x}) = \mathbf{x}'$ aims to maintain the desired inference accuracy, i.e., $P(U|\mathbf{x}) \approx P(U|\mathbf{x}')$, while reducing the intrusive inference accuracy to near random guessing level, i.e., $P(S|\mathbf{x}') \approx P_{\text{guess}}$. Note that CLOAK does not require knowledge of the intrusive inference model or the desired inference model used by the HBC service provider.

Note that the inherent trade-off between privacy and utility implies that any transformation $f(\mathbf{x}) = \mathbf{x}'$ intended to make $P(S|\mathbf{x}')$ close to random guessing would inevitably reduce utility, i.e. $P(U|\mathbf{x}) > P(U|\mathbf{x}')$, and vice versa.

IV. METHODOLOGY

A. Background on Latent Diffusion Models

Diffusion models are a class of (probabilistic) generative models that have shown extraordinary success in the image domain, outperforming GAN-based approaches [27], [28]. Diffusion models consist of a forward process that gradually adds Gaussian noise through T timesteps to corrupt the data, and a backward process that reverses this process to generate realistic data from noise. Given a data point $\mathbf{x}_0 \sim q(\mathbf{x}_0)$, the forward diffusion process perturbs the data at timestep t using noises sampled following a variance scheduler β_t , where $0 < \beta_1 < \dots < \beta_T < 1$. DDPM [28] models the diffusion process as Markovian:

$$q(\mathbf{x}_t|\mathbf{x}_{t-1}) = \mathcal{N}(\mathbf{x}_t; \sqrt{1 - \beta_t}\mathbf{x}_{t-1}, \beta_t\mathbf{I}), \quad (1)$$

where \mathbf{x}_t is dependent on \mathbf{x}_{t-1} , requiring the sampling process to iterate through all T timesteps. To simplify the sampling process, one can rewrite (1) by defining $\alpha_t = 1 - \beta_t$, and $\bar{\alpha} = \prod_{t=1}^T \alpha_t$:

$$q(\mathbf{x}_t|\mathbf{x}_0) = \mathcal{N}(\mathbf{x}_t; \sqrt{\bar{\alpha}_t}\mathbf{x}_0, (1 - \bar{\alpha}_t)\mathbf{I}), \quad (2)$$

where $\mathbf{x}_t = \sqrt{\bar{\alpha}_t}\mathbf{x}_0 + \sqrt{1 - \bar{\alpha}_t}\epsilon_0$ can be derived by applying the reparameterization trick, $\epsilon \sim \mathcal{N}(0, \mathbf{I})$. A neural network $\epsilon_\theta(\mathbf{x}_t, t)$ is trained to approximate the intractable $q(\mathbf{x}_{t-1}|\mathbf{x}_t)$ and predict the noise ϵ added at each timestep. The loss function for training $\epsilon_\theta(\mathbf{x}_t, t)$ is the mean squared error (MSE) given below:

$$\mathcal{L}_\theta = \|\epsilon - \epsilon_\theta(\mathbf{x}_t, t)\|_2^2 = \|\epsilon - \epsilon_\theta(\sqrt{\bar{\alpha}_t}\mathbf{x}_0 + \sqrt{1 - \bar{\alpha}_t}\epsilon, t)\|_2^2, \quad (3)$$

where t is the timestep, $\epsilon \sim \mathcal{N}(0, \mathbf{I})$.

Latent diffusion models (LDMs) [21] extend diffusion models by performing data generation in the latent space \mathcal{Z} , which can be obtained using an autoencoder. The low-dimensional latent space allows LDMs to focus on semantic embeddings extracted from the original data and is more efficient to compute.

We train a VAE, comprised of an encoder \mathcal{E} and a decoder \mathcal{D} , to learn the latent space \mathcal{Z} . The latent representation learned by the VAE, denoted as \mathbf{z} , can be expressed as [29]:

$$\mathbf{z} = \mu(\mathbf{x}; \mathcal{E}) + \epsilon \odot \exp\left(\frac{\sigma(\mathbf{x}; \mathcal{E})}{2}\right), \quad \epsilon \sim \mathcal{N}(\mathbf{0}, \mathbf{I}), \quad (4)$$

where μ and σ are the mean and log-covariance of the learned multi-variate Gaussian distribution representing the latent distribution of data \mathbf{x} . Following existing literature [21], we only use the deterministic posterior generated by the encoder \mathcal{E} as the latent representation for the LDM, i.e., $\mathbf{z} = \mu(\mathbf{x}; \mathcal{E})$. This is because the forward diffusion process already introduces stochasticity, so sampling from the latent distribution can further introduce noise and degrade the quality of data generated by the LDM. We train a neural network $\epsilon_\theta(\mathbf{x}_t, t)$ to approximate the intractable $q(\mathbf{x}_{t-1}|\mathbf{x}_t)$ and predict the noise ϵ added at each timestep. The LDM's loss function can be written as:

$$\mathcal{L}_\theta = \|\epsilon - \epsilon_\theta(\mathbf{z}_t, t)\|_2^2 = \|\epsilon - \epsilon_\theta(\sqrt{\bar{\alpha}_t}\mathbf{z}_0 + \sqrt{1 - \bar{\alpha}_t}\epsilon, t)\|_2^2, \quad (5)$$

where β is the noise scheduler, and $\mathbf{z}_t = \mathcal{E}(\mathbf{x}_t)$. Optimizing (5) allows the LDM to output generated data \mathbf{z}'_t in the latent space. The decoder \mathcal{D} then maps \mathbf{z}'_t to the input space, i.e., $\mathbf{x}'_t = \mathcal{D}(\mathbf{z}'_t)$. The VAE is pre-trained on the raw sensor data.

B. Contrastive Classifier-Free Guidance for Positive Conditioning

Let $\mathbf{x} \sim \mathbf{D}$ be a sensor data (time-series) segment, a neural network encoder $\phi : \mathcal{X} \rightarrow \mathcal{Z}_U$ maps each input to a latent representation $\mathbf{z}_U = \phi(\mathbf{x})$. Our goal is to learn representations that contain maximum information about U , while being independent of S . To this end, the encoder ϕ is trained using contrastive learning. We condition the LDM with the contrastively learned \mathbf{z}_U via classifier-free guidance, hence we denote our conditioning method as Contrastive Classifier-free Guidance (CCFG). We consider \mathbf{x} as the anchor point, and define the positive/negative sample $\mathbf{x}^+/\mathbf{x}^-$ as any data point in \mathbf{D} that shares the same/different public attribute class as the anchor point \mathbf{x} , respectively, i.e., $U_{\mathbf{x}^+} = U_{\mathbf{x}}$, $U_{\mathbf{x}^-} \neq U_{\mathbf{x}}$. Note that for both positive and negative samples, their corresponding private attribute classes may differ from the anchor point's private attribute class. We use the InfoNCE loss denoted as $\mathcal{L}_{\text{InfoNCE}}(\mathbf{x})$ and defined below:

$$-\log \frac{\exp(S(\mathbf{z}_U, \mathbf{z}_U^+)/\tau)}{\exp(S(\mathbf{z}_U, \mathbf{z}_U^+)/\tau) + \sum_{j=1}^K \exp(S(\mathbf{z}_U, \mathbf{z}_{U^-_j})/\tau)}, \quad (6)$$

where \mathbf{z}_U^+ and $\mathbf{z}_{U^-_j}$ are latent representations extracted from positive samples \mathbf{x}^+ and negative samples \mathbf{x}_j^- , respectively; K is the number of negative samples used; $S(u, v) = \frac{u^\top v}{\|u\| \|v\|}$ is the cosine similarity and τ is the temperature controlling the similarity measurement sensitivity.

The InfoNCE loss approximates a lower bound on the mutual information (MI) $I(\mathbf{z}_U; U)$ [16]. Thus, minimizing it encourages the encoder ϕ to learn a representation \mathbf{z}_U that encodes discriminative information about the public attribute

U . Once the encoder is trained, for every data point, we first extract $\mathbf{z}_U = \phi(\mathbf{x})$, and then apply classifier-free guidance [30] to condition the LDM towards generating data that maintains information about the public attribute U . Following Ho and Salimans [30], we define our noise predictor ϵ_θ as:

$$\bar{\epsilon}_\theta(\mathbf{z}_t, t, \mathbf{z}_U) = (1 + w_U)\epsilon_\theta(\mathbf{z}_t, t, \mathbf{z}_U) - w_U\epsilon_\theta(\mathbf{z}_t, t), \quad (7)$$

where w_U is the weight controlling the strength of conditioning the public attribute U , $\epsilon_\theta(\mathbf{z}_t, t, \mathbf{z}_U)$ is the score estimator for the LDM conditioned on the contrastively learned \mathbf{z}_U , $\epsilon_\theta(\mathbf{z}_t, t) = \epsilon_\theta(\mathbf{z}_t, t, \emptyset)$ is the score estimator for the unconditioned LDM by setting \mathbf{z}_U to zero. CCFG then applies Adaptive Group Normalization (AdaGN) [27] to condition the LDM on \mathbf{z}_U .

1) *Implicit Disentanglement via Contrastive Sampling*: We now provide the intuition for why $I(\mathbf{z}_U; S)$ is minimized when maximizing $I(\mathbf{z}_U; U)$. Our explanation relies on two practical assumptions: 1) the training dataset contains diverse samples, so that there exist many positive pairs $(\mathbf{x}, \mathbf{x}^+)$ that share the same U but differ in S ; 2) the public and private attributes are not strongly correlated, allowing for at least partial disentanglement between them.

Our sampling strategy ensures that positive pairs $(\mathbf{x}, \mathbf{x}^+)$ are selected solely based on the shared public attribute U , irrespective of their private attribute S . Thus, samples with the same U but different S must map to nearby representations, discouraging ϕ from encoding information about S in \mathbf{z}_U . As a result, the conditional distribution $p(\mathbf{x}^+ | \mathbf{x}, U_{\mathbf{x}^+} = U_{\mathbf{x}})$ will become marginal over S , implying a conditional independence relationship in the latent space, i.e. $\phi(\mathbf{x}) \perp S | U$. Thus, training ϕ minimizes the conditional MI ($\min_\phi I(\mathbf{z}_U; S | U)$) implicitly.

If $I(\mathbf{z}_U; S | U)$ becomes small (ideally approaching 0), then \mathbf{z}_U contains almost no information about S given U . Thus, minimizing the InfoNCE loss with our sampling strategy leads to representations \mathbf{z}_U that are (i) highly informative of the public attribute U , and (ii) almost independent of the private attribute S , thereby encouraging disentanglement in the latent space. In addition, we note that training the encoder ϕ does not require prior knowledge of the private attribute S . Therefore, the encoder will learn to disentangle the public attribute from other attributes. This *white-listing characteristic* allows CLOAK to extend the privacy protection to unspecified attributes R .

C. Enabling Flexible Privacy Protection via Negated Classifier Guidance

We condition the LDM-based obfuscation model on the private attribute following the idea of classifier guidance [27]. This decouples conditioning of the private attribute from the training process, deferring it to the sampling stage. We note that the LDM-based obfuscation model is still conditioned on the public attribute during training, which is acceptable as the public attribute is assumed to be fixed.

Unlike conventional classifier guidance, which is typically used to guide a diffusion model towards adding information

about the condition, we use negated classifier guidance such that information about the conditioned private attribute is excluded in the generated data. Specifically, we apply negated classifier guidance on top of the conditional diffusion model guided by the public attribute U . We denote the negated private attribute as \bar{S} , i.e., the complement of S , and the classifier trained for conditioning the private attribute as the auxiliary privacy model η (shown in Figure 1). More specifically, \bar{S} is all private attribute classes in the dataset except the user's actual private attribute class. Following Dong et al. [31] and Liu et al. [32], we can write:

$$p_{\theta, \phi, \eta}(\mathbf{z}_t | U, \bar{S}) \propto p_\theta(\mathbf{z}_t) \frac{p_\phi(U | \mathbf{z}_t)}{p_\eta(\bar{S} | U, \mathbf{z}_t)}. \quad (8)$$

Notice that U and S may not be completely disentangled, so we cannot further simplify $p_\eta(S | U, \mathbf{z}_t)$. Computing the gradient of the log of (8) yields:

$$\begin{aligned} \nabla_{\mathbf{z}_t} \log (p_\theta(\mathbf{z}_t) p_\phi(U | \mathbf{z}_t) p_\eta(\bar{S} | U, \mathbf{z}_t)) = \\ -\frac{\epsilon_\theta(\mathbf{z}_t)}{\sqrt{1 - \bar{a}_t}} + \nabla_{\mathbf{z}_t} \log p_\phi(U | \mathbf{z}_t) - \nabla_{\mathbf{z}_t} \log p_\eta(S | U, \mathbf{z}_t), \end{aligned} \quad (9)$$

This allows writing $\bar{\epsilon}_\theta(\mathbf{z}_t, t, U, S)$ used for sampling as:

$$\begin{aligned} \bar{\epsilon}_\theta(\mathbf{z}_t, t, U, S) = (1 + w_U)\epsilon_\theta(\mathbf{z}_t, t, \mathbf{z}_U) - w_U\epsilon_\theta(\mathbf{z}_t, t) \\ + w_S \sqrt{1 - \bar{a}_t} \nabla_{\mathbf{z}_t} \log p_\eta(S | \mathbf{z}_U, \mathbf{z}_t), \end{aligned} \quad (10)$$

where w_U and w_S are weights that control the strength of the positive condition and negative condition, resp. To obtain $p_\eta(S | \mathbf{z}_U, \mathbf{z}_t)$, we concatenate the latent representation \mathbf{z}_U with the input of the first FC layer in η . η must be trained on noisy inputs to consume perturbed \mathbf{z}_t at the sampling stage. To overcome this challenge, we further apply universal guidance [33] to allow training η on clean data. During the sampling, classifier guidance will be applied to clean data $\hat{\mathbf{z}}_0$ generated by the diffusion model conditioned on the public attribute, rather than the noisy data \mathbf{z}_t . We express $\hat{\mathbf{z}}_0$ as:

$$\begin{aligned} \hat{\mathbf{z}}_0 &= \frac{\mathbf{z}_t - \sqrt{1 - \bar{a}_t} \bar{\epsilon}_\theta(\mathbf{z}_t, t, \mathbf{z}_U)}{\sqrt{\bar{a}_t}} \\ &= \frac{\mathbf{z}_t - \sqrt{1 - \bar{a}_t} ((1 + w_U)\epsilon_\theta(\mathbf{z}_t, t, \mathbf{z}_U) - w_U\epsilon_\theta(\mathbf{z}_t, t))}{\sqrt{\bar{a}_t}}. \end{aligned} \quad (11)$$

We can then update our noise prediction model as:

$$\begin{aligned} \bar{\epsilon}_\theta(\mathbf{z}_t, t, U, S) = (1 + w_U)\epsilon_\theta(\mathbf{z}_t, t, \mathbf{z}_U) - w_U\epsilon_\theta(\mathbf{z}_t, t) \\ + w_S \sqrt{1 - \bar{a}_t} \nabla_{\mathbf{z}_t} \log p_\eta(S | \mathbf{z}_U, \hat{\mathbf{z}}_0). \end{aligned} \quad (12)$$

V. EXPERIMENTS

A. Datasets

We use four publicly available time-series datasets, MobiAct [34], MotionSense [1], WiFi-HAR [35], and AudioMNIST [36], covering different sensing modalities (i.e. motion, WiFi channel state information, and audio) for evaluation. To ensure fairness and consistency, we use the same data selection strategy and pre-processing steps introduced in prior work on data obfuscation. Specifically, we follow [4], [5] for MobiAct, MotionSense, and WiFi-HAR; we follow [10] for

AudioMNIST. In addition to sensor-generated (time-series) data, we demonstrate the efficacy of CLOAK for obfuscating facial images on an image dataset.

1) *MobiAct* [34]: It is a human activity recognition (HAR) dataset collected using motion sensors (accelerometer, gyroscope, and orientation sensors) embedded in a smartphone. We use the motion data of 36 participants performing 4 different activities: walking, standing, jogging, and walking upstairs. We select the data collected from the 3-axis accelerometer and the 3-axis gyroscope, resulting in 6 channels of sensor readings (time-series). The data is standardized and segmented using a sliding window of size 128 samples with a stride length of 10 samples. We define the subject's activity as the public attribute. We consider 2 private attributes: their gender and weight, where gender contains 2 classes in this case (male, female), and weight contains 3 classes: $\leq 70\text{kg}$, $70\text{-}90\text{kg}$, and $\geq 90\text{kg}$. We split the data into training and testing sets with a ratio of 8:2.

2) *MotionSense* [1]: It is another HAR dataset containing motion data collected by the accelerometer and gyroscope in a smartphone. We use the motion data of 24 participants performing 4 different activities: walking upstairs, walking downstairs, walking, and jogging. We consider the subject's activity as the public attribute. Each activity is repeated 15 times, where the first 9 repeats are used for training and the remaining 6 are used for testing. We consider the binary gender attribute as the private attribute. We aggregate the magnitude of accelerometer/gyroscope readings over the 3 axes of each sensor, respectively. This creates a 2-channel sensor data, which is then segmented using the same sliding window as the MobiAct dataset.

3) *WiFi-HAR* [35]: This dataset contains WiFi channel state information—a radio frequency-based wireless sensing modality—which can be used to detect human activity. We select the data captured by 3 line-of-sight transceiver pairs, comprising 1 transmitter and 3 receivers, where each transceiver pair generates data of 30 channels. Hence, the captured data contains a total of 90 channels. We compute the magnitude of channel state information (CSI) for each channel and perform standardization. A sliding window of size 80 samples with a hop size of 40 samples is applied to perform data segmentation. We use the data collected by 10 subjects performing 4 activities: standing, sitting, lying down, and turning around. Each activity is repeated 20 times. We consider the subject's activity as the public attribute and their weight as the private attribute, where weight is categorized into two classes ($\geq 80\text{kg}$ and $< 80\text{kg}$). The data is randomly shuffled and divided into training/test set with a ratio of 8:2.

4) *AudioMNIST* [36]: This audio dataset contains recordings of spoken digits from 0-9 in English. Recordings from 60 participants are included. We use HuBERT-B [37] to convert the audio signals into feature embeddings, then rescale the embeddings so that their L2-norm equals 1, following MaSS [10]. We consider the public attribute to be the digit spoken. We consider the subject's gender (2 classes) as the private attribute, and their age (18 classes), accent (16 classes),

and user ID (60 classes) as unspecified attributes. The train-test split ratio is 8:2.

5) *Adience* [38]: This is a facial image dataset used for benchmarking age and gender classification models. We use the aligned faces, a total of 19975 images of 33 subjects. We convert images to grayscale and resize them to 80×80 . We then perform normalization to ensure all pixel values are within the range of 0 to 1. We use a 7:3 ratio to randomly sample the training and testing sets. We consider the 33-class user ID as the public attribute. We consider two private attributes: the user's gender (binary) and the user's age, which is categorized into 8 groups: 0-3, 4-6, 8-13, 15-20, 22-32, 35-48, 48-58, 60-100.

For the Adience dataset, we use a CNN-based VAE, where the encoder contains three batch-normalized convolutional layers. For the encoder, the number of kernels, kernel size, step size, and padding used for each layer are $(128, 5, 5, 0)$, $(256, 3, 1, 1)$, $(512, 3, 1, 1)$, resp. The outputs of the third convolutional layer are fed to two convolutional layers of $(8, 3, 1, 1)$ to output the mean and log variance of the latent distribution. This maps the grayscale 80×80 image into latent representations with a dimension of $8\times 16\times 16$. We use 3×3 convolutional kernels in the UNet to replace the 1×3 kernels used for time-series data. We use the same hyperparameters, $w_U = 6$, $w_S = 0.5$, to obtain the results presented in this section.

B. Evaluation Metrics

1) *Privacy Loss*: The adversary performs an attribute inference attack to infer private attributes from the shared data, which might be obfuscated. We define the privacy loss L_S as the deviation of the classification accuracy of an intrusive inference model (M_S) that predicts the private attributes from the obfuscated data from random guessing:

$$L_S = |Acc(M_S) - Acc(\text{guess})|, \quad Acc(\text{guess}) = 1/\text{card}(S),$$

where $Acc(M_S)$ is the classification accuracy of the intrusive inference model on the private attribute S , $Acc(\text{guess})$ is the random guessing accuracy (assuming the adversary does not know the true distribution of private attribute classes), and $\text{card}(S)$ is the cardinality of the set of private attribute classes. We use a CNN that contains four convolutional layers followed by three fully connected layers as the intrusive inference model. This model is pre-trained on the raw sensor data to predict the private attributes. While an adversary could adopt a different architecture, we use this model as a representative example, as it achieves high accuracy on the raw data. An ideal data obfuscation model should reduce the average intrusive inference accuracy to near the random guessing level; thus, a lower L_S is better. For datasets that contain unspecified attributes R , we train intrusive inference models M_R in a similar way.

2) *Data Utility*: The classification accuracy of a desired inference model M_U that predicts the public attribute from the obfuscated data is used as a measure of utility. Our desired inference model has the same architecture as the intrusive

inference model described above. We pre-train M_U on raw sensor data. Ideally, a data obfuscation model should generate obfuscated data that maintains the utility of raw data.

C. Implementation

We pre-train the VAE used in CLOAK to transform the sensor data between its original data space and the latent space. The VAE is implemented using a symmetric encoder and decoder using fully connected (FC) layers, where the encoder comprises 4 FC layers with 2048, 2048, 1024, and 512 neurons, resp. The mean and log variance of the latent representation are generated using FC layers with 60 neurons (i.e., dimension of the latent space). We implement the diffusion model using the UNet [39] architecture and adopt a linear schedule from 0.0001 to 0.02 with $T=1000$. We modify the 2D 3×3 convolutional kernels used in the UNet to 1×3 to work with 1D latent representations. We use DDIM [40] as the sampling strategy with 50 sampling steps. For all datasets, we implement the contrastive encoder ϕ using a CNN that contains 2 convolutional layers followed by 3 FC layers; We implement the auxiliary privacy model η using 5 FC layers. We train ϕ on raw sensor data and η on the latent representation extracted by the VAE’s encoder. We implement CLOAK using PyTorch 2 and train it on a server with Ubuntu 20.04, equipped with an Intel Core i9-9940X CPU, 128 GB RAM, and 1 RTX 2080 Ti GPU. Our implementation will be made publicly available on GitHub upon acceptance.

D. Training Details and Hyperparameter Selection

We train the VAE used in CLOAK using the AdamW optimizer with a learning rate of 0.001. We set the weight for the KL divergence loss to $1e^{-7}$ for AudioMNIST, and $1e^{-6}$ for all other datasets. We train both the contrastive encoder ϕ and auxiliary privacy model η using the Adam optimizer with a learning rate of $2e^{-4}$. The UNet is trained with the AdamW optimizer with a cosine annealing scheduler that has an initial learning rate of $2e^{-4}$. We set the training epochs for MotionSense, MobiAct, WiFi-HAR, and AudioMNIST to 80, 28, 80, and 120, resp. CLOAK uses two hyperparameters w_U and w_S to navigate the privacy-utility trade-offs. We set w_U and w_S empirically through grid search. For MotionSense, WiFi-HAR, and AudioMNIST datasets, we set (w_U, w_S) to $(4.5, 0.008)$, $(6, 0.005)$, and $(2, 0.07)$, resp. For both gender and weight obfuscation on MobiAct, we set (w_U, w_S) to $(4, 0.05)$.

E. Baselines

We consider three generative obfuscation models as baselines, and use the code released by the authors to evaluate them.

1) *ObscureNet* [4]: is a GAN-based obfuscation model that has been shown to outperform prior GAN-based obfuscation models. It uses a conditional VAE (CVAE) to reconstruct sensor data and employs a discriminator to remove information about private attributes from the latent space learned by the CVAE. We use the randomized anonymization scheme

proposed by the authors, as it aligns with our evaluation metric and is robust to re-identification attacks. We compare with ObscureNet on MobiAct, MotionSense, and WiFi-HAR. Since ObscureNet requires training a dedicated obfuscation model for each public attribute class, it is costly to train it on AudioMNIST, which contains 10 classes for the public attribute (digit).

2) *MaSS* [10]: is an obfuscation model that preserves information about both user-annotated public attributes U and unannotated attributes R , while protecting private attributes S . It integrates adversarial training, mutual information minimization, and contrastive learning, achieving strong performance over several baselines. However, MaSS makes two assumptions that limit its practicality: 1) downstream applications have access to the obfuscated data and the correct labels for U and R to fine-tune M_U and M_R , whereas CLOAK does not require changing these models. 2) data utility with respect to R should be maintained, whereas CLOAK aims to protect R because it may be deemed private in the future. Hence, the results on unspecified attributes R are not directly comparable between MaSS and CLOAK.

MaSS is evaluated using an M_U that is fine-tuned for 100 epochs on the obfuscated training dataset and correct labels for U , using the same setting as the initial training of M_U . We compare with MaSS on MotionSense and AudioMNIST, as its implementation is available for these datasets only.

3) *PrivDiffuser* [5]: is a state-of-the-art diffusion-based obfuscation model. It trains a diffusion model that operates in the original data space and conditions it on the public attribute using latent representations extracted by a surrogate utility model. Classifier guidance is used to condition the private attribute via an auxiliary privacy classifier. PrivDiffuser disentangles public and private attributes by minimizing the estimated mutual information. We compare with PrivDiffuser on MobiAct, MotionSense, and WiFi-HAR. PrivDiffuser uses 2D convolutional kernels, which do not work for the 1D AudioMNIST dataset.

F. Evaluation of Data Obfuscation Performance

We evaluate obfuscation models on 4 time-series datasets and report average and standard deviation across 5 runs in Table II. Our result shows that sharing raw sensor data leads to high privacy loss on all datasets, underscoring the need for obfuscation.

Comparison with MaSS: MaSS has the worst privacy loss among the baselines. On MotionSense and AudioMNIST, the privacy loss only decreases by 36.64% and 42.02%, respectively, relative to the raw data. Despite fine-tuning M_U for MaSS, it still underperforms CLOAK by 17.30% and 1.09% in terms of utility on MotionSense and AudioMNIST, respectively. Without fine-tuning M_U , the utility of the obfuscated data is severely degraded on both datasets. In particular, without fine-tuning, it yields 15.83% accuracy for activity recognition on MotionSense, and 10.28% accuracy for inferring the pronounced digit on AudioMNIST, effectively rendering the obfuscated data unusable for downstream applications. It is

TABLE II

CLOAK’S OBFUSCATION PERFORMANCE COMPARED TO BASELINES ON MOTIONSENSE, MOBIACT, WiFi-HAR, AND AUDIOMNIST. RESULTS PRESENTED AS MEAN \pm STD OVER 5 RUNS. UNDERSCORED NUMBERS ARE THE BEST RESULTS WITH STATISTICAL SIGNIFICANCE ($P<0.05$) ACCORDING TO A TWO-SIDED PAIRED T-TEST FOR MOTIONSENSE AND A TWO-SIDED INDEPENDENT T-TEST FOR OTHER DATASETS.

Dataset	Method	Accuracy / F1 Score (%)		Privacy Loss L_S (% deviation from random guessing)	
		Public Attribute- U	Private Attribute- S	Unspecified Attributes- R	
MotionSense	Raw Data	97.47 \pm 0.00 / 96.59 \pm 0.00	43.52 \pm 0.00	-	
	MaSS	79.90 \pm 2.62 / 63.76 \pm 1.97	6.88 \pm 0.22	-	
	ObscureNet	94.96 \pm 0.33 / 93.05 \pm 0.56	3.46 \pm 0.33	-	
	PrivDiffuser	96.32 \pm 0.56 / 95.69 \pm 0.57	0.04 \pm 0.86	-	
	CLOAK	97.20 \pm 0.20 / 96.28 \pm 0.31	0.02 \pm 0.56	-	
		Activity (\uparrow)	Gender (\downarrow)	Weight (\downarrow)	
MobiAct	Raw Data	98.87 \pm 0.00 / 92.04 \pm 0.01	47.51 \pm 0.00	58.41 \pm 0.00	
	ObscureNet	97.18 \pm 0.42 / 84.80 \pm 1.32	2.18 \pm 0.42	39.06 \pm 1.17	
	PrivDiffuser	97.40 \pm 0.20 / 85.49 \pm 0.64	1.43 \pm 0.53	16.11 \pm 1.11	
	CLOAK	98.24 \pm 0.09 / 88.25 \pm 0.69	0.06 \pm 0.61	8.58 \pm 1.25	
		Activity (\uparrow)	Weight (\downarrow)	Gender (\downarrow)	
WiFi-HAR	Raw Data	98.87 \pm 0.00 / 92.04 \pm 0.01	58.41 \pm 0.00	47.51 \pm 0.00	
	ObscureNet	96.97 \pm 0.28 / 84.33 \pm 1.15	4.72 \pm 0.49	10.96 \pm 0.59	
	PrivDiffuser	97.03 \pm 0.39 / 84.17 \pm 1.27	2.45 \pm 1.73	9.40 \pm 1.28	
	CLOAK	98.24 \pm 0.09 / 88.16 \pm 0.76	0.14 \pm 0.42	0.77 \pm 2.18	
		Activity (\uparrow)	Weight (\downarrow)	-	
AudioMNIST	Raw Data	97.83 \pm 1.10 / 97.83 \pm 1.16	49.13 \pm 0.11	-	
	ObscureNet	86.37 \pm 1.33 / 86.17 \pm 1.32	1.43 \pm 0.68	-	
	PrivDiffuser	88.18 \pm 1.37 / 88.12 \pm 1.41	0.79 \pm 2.26	-	
	CLOAK	95.39 \pm 1.30 / 95.39 \pm 1.30	0.18 \pm 0.38	-	
		Digit (\uparrow)	Gender (\downarrow)	Age (\downarrow)	Accent (\downarrow)
	Raw Data	98.92 \pm 0.02 / 98.92 \pm 0.02	48.12 \pm 0.02	89.60 \pm 0.07	89.05 \pm 0.03
	MaSS	97.72 \pm 0.26 / 97.72 \pm 0.26	6.10 \pm 0.32	-	-
	CLOAK	98.81 \pm 0.37 / 98.80 \pm 0.37	0.34 \pm 0.35	3.19 \pm 0.26	47.35 \pm 0.86
					User ID (\downarrow)
					0.51 \pm 0.04

worth noting that MaSS does not protect unspecified attributes R (it rather does the opposite), hence the privacy loss is not reported for these attributes on AudioMNIST. CLOAK offers reasonable protection for all unspecified attributes without requiring prior knowledge of R . The relatively higher privacy loss for the accent attribute is primarily due to the model misclassifying most samples as the dominant class. We note that the average F1 score for intrusive inference on accent is only 5.82%, indicating that the adversary cannot obtain meaningful information on accent from the data obfuscated by CLOAK.

Comparison with ObscureNet: ObscureNet, which is a GAN-based obfuscation model, achieves a good privacy-utility trade-off on MotionSense, MobiAct, and WiFi-HAR. However, it consistently underperforms the two diffusion-based models—PrivDiffuser and CLOAK—in terms of data utility and privacy loss on all four time-series datasets. Moreover, in the MobiAct dataset, it cannot successfully protect the unspecified attribute. When performing gender obfuscation on MobiAct, for the unspecified weight attribute, ObscureNet reduces the privacy loss by 19.35% compared to the raw data, while CLOAK reduces the privacy loss by 49.83%. Similarly, ObscureNet yields the highest privacy loss on the unspecified gender attribute when performing weight obfuscation

on MobiAct. It is also worth noting that ObscureNet must be retrained to protect different private attributes, whereas the contrastive encoder and the diffusion model in CLOAK only need to be trained once and can protect different private attributes by introducing the corresponding auxiliary privacy model during sampling. Apart from these, ObscureNet has a major drawback: it requires training a dedicated model for each public attribute class, significantly increasing the training cost.

Comparison with PrivDiffuser: CLOAK achieves comparable privacy loss to PrivDiffuser for the gender attribute on MotionSense, while delivering significantly higher activity recognition accuracy and F1 score. On MobiAct and WiFi-HAR, CLOAK consistently provides the highest data utility with statistical significance. Notably, on WiFi-HAR, PrivDiffuser can only achieve $\sim 88\%$ activity recognition accuracy given that identifying human activity from radio frequency signals is inherently more challenging. Yet, CLOAK drastically improves the activity recognition accuracy and F1 score by respectively 7.21% and 7.27%, on average, over PrivDiffuser. This is while CLOAK achieves the lowest privacy loss on both datasets, significantly outperforming PrivDiffuser.

Considering the unspecified attribute in MobiAct, CLOAK reduces privacy loss by 7.53% compared to PrivDiffuser

when performing gender obfuscation. When obfuscating the weight attribute, CLOAK reduces the privacy loss by 8.63% than PrivDiffuser. This highlights the superior disentanglement achieved by the proposed CCFG compared to the mutual information-based regularization used in PrivDiffuser. Overall, CLOAK consistently achieves the best privacy-utility trade-offs across all time-series datasets.

G. Protecting Attributes in Images

We now evaluate CLOAK’s obfuscation capability on images from the Adience dataset, reporting privacy-preserving performance averaged over 5 runs in Table III. For comparison, we include the results of MaSS for suppressing the gender and age attributes, respectively, while treating the remaining attributes as unannotated useful attributes. Because the authors’ implementation of MaSS for Adience is unavailable, we were unable to reproduce its results despite our best efforts. Instead, we directly compare with the values reported in [10] and denote them as MaSS* to clarify that the data points and evaluation models used in that study may differ from ours. Finally, we omit the accuracy for the unspecified attribute because MaSS* is designed to retain, rather than suppress, information about that attribute.

In the case of gender obfuscation, it is evident that CLOAK can effectively reduce the privacy loss on the gender attribute to a random guessing level. This comes at the cost of a slight decrease (2.39%) in data utility. For the unspecified age attribute, the privacy loss is reduced by 45.24%. This suggests a stronger entanglement between the user ID and the respective age group. Although there is a gap between the privacy loss on the unspecified age attribute and the random guessing level, the result is encouraging given that this level of protection is provided due to the white-listing characteristic of diffusion-based obfuscation, without requiring any prior knowledge of the user’s age. MaSS* achieves 72.55% accuracy for user ID classification, which is $\sim 24\%$ lower than CLOAK, meanwhile its privacy loss is $\sim 2\%$ worse than CLOAK.

In the case of age obfuscation, CLOAK yields 84.22% accuracy for user ID classification and 20.40% privacy loss for the age attribute. We attribute this higher privacy loss to the stronger entanglement between user ID and age, which results in a less favorable trade-off, and corroborate this in the next paragraph. Nevertheless, CLOAK provides strong privacy protection for the unspecified gender attribute, yielding a privacy loss of only 2.64%. The results of MaSS* likewise indicate a poorer privacy-utility trade-off when suppressing the age attribute, yielding only 50.05% desired inference accuracy on the ID attribute, underperforming CLOAK by approximately 29%. Although MaSS* exhibits about 4% lower privacy loss for the age attribute, CLOAK still delivers a substantially better balance between privacy and utility.

Effect of Public and Private Attribute Entanglement on the Privacy–Utility Trade-off: Table III shows that data utility decreases substantially, and privacy loss for the private attribute increases substantially when the private attribute is age compared to when it is gender. To validate that this effect

TABLE III
GENDER AND AGE OBFUSCATION RESULTS ON ADIENCE; PUBLIC ATTRIBUTE IS USER ID. FOR MASS*, WE REPORT RESULTS FROM [10] FOR GENDER AND AGE SUPPRESSION, RESPECTIVELY, WHILE THE REMAINING TWO ATTRIBUTES ARE UNANNOTATED USEFUL ATTRIBUTES.

Metric	Privacy Loss L_S (%)			
	Attribute	U -ID (\uparrow)	S -Gender (\downarrow)	R -Age (\downarrow)
Raw Data		99.00 ± 0.10	49.86 ± 0.04	87.38 ± 0.04
MaSS*		72.55	2.40	-
CLOAK		96.61 ± 0.32	0.09 ± 0.48	42.14 ± 0.58
Attribute	Privacy Loss L_S (%)			
	U -ID (\uparrow)	S -Age (\downarrow)	R -Gender (\downarrow)	
Raw Data		99.00 ± 0.10	87.38 ± 0.04	49.86 ± 0.04
MaSS*		50.05	16.42	-
CLOAK		84.22 ± 1.29	20.40 ± 1.78	2.64 ± 0.90

arises from the stronger entanglement between the public attribute (user ID) and age than between the public attribute and gender, we train two MINE [41] models to estimate the MI between user ID and gender, and the MI between user ID and age. We repeat the experiments five times and report the average MI. We find that the average MI between ID and gender is 0.097, whereas the average MI between ID and age is 0.872. This indicates that the correlation between the public attribute and age is indeed much stronger than the correlation with gender, confirming that stronger entanglement can result in a worse privacy–utility trade-off.

Visualization of Obfuscated Images: In Figure 2 and 3, we provide a comparison between images before and after gender and age obfuscation, respectively, where the first row shows the original images, and the second row shows the obfuscated ones. For all illustrated images, the desired inference model successfully predicts the correct user ID given the obfuscated images, whereas the intrusive inference model predicts the wrong private attribute class in all cases. Looking closely at the obfuscated images, we find that CLOAK preserves salient facial characteristics of the user, which are highly associated with their identity. We also find that the obfuscated images tend to borrow features from the real images of other users in the training set for unspecified attributes, such as hairstyle, age/gender, and background. Thus, unspecified attributes can be protected to a reasonable extent, as long as the training set contains sufficient samples with diverse classes. We also note that the images generated by CLOAK have significantly better quality than the images generated by MaSS (cf. Figure 4 in [10]). This visualization concurs with the intuition that diffusion-based obfuscation models can protect unspecified attributes by leveraging the inherent stochasticity of sampling in the generative process.

H. Adjusting Privacy–Utility Trade-offs

CLOAK allows users to navigate the privacy-utility trade-off by tuning two hyperparameters, w_U and w_S , without retraining. We demonstrate this for the MotionSense dataset, using activity as the public attribute and gender as the private attribute. Figure 4 shows the average desired inference accuracy versus the average intrusive inference accu-



Fig. 2. Illustration of gender obfuscation on Adience. User ID is the public attribute, age is an unspecified attribute. First row: original images, second row: obfuscated images with the opposite gender detected by the intrusive inference model. Each column is a pair of images before and after obfuscation.



Fig. 3. Illustration of age obfuscation on Adience. User ID is the public attribute, gender is an unspecified attribute. First row: original images, second row: obfuscated images with a different age group detected by the intrusive inference model. Each column is a pair of images before and after obfuscation.

racy. The trade-off curves are obtained from a pre-trained CLOAK model using a combination of $w_U \in [1, \dots, 9]$ and $w_S \in [0, 0.03, 0.06, 0.09]$. The red star denotes the ideal trade-off where the activity recognition accuracy on obfuscated data remains at the same level as raw data and the gender recognition accuracy is at the random guessing level.

For a fixed w_S , increasing w_U significantly improves data utility until it reaches 6. However, stronger positive conditioning (higher w_U) also increases the intrusive inference accuracy by inevitably including some information about private attributes, as the attributes are not fully disentangled. A stronger negative conditioning would be required in this case to balance data utility and privacy.

Fixing w_U and increasing w_S drastically reduces intrusive inference accuracy, highlighting the effectiveness of negative conditioning in removing information about the user's private attribute class. In particular, when $w_S = 0$, privacy protection relies solely on CLOAK's white-listing characteristic, resulting in higher intrusive inference accuracy than when $w_S > 0$. Moreover, we find that increasing w_S has a limited impact on the activity recognition accuracy, which further confirms that negated classifier guidance can effectively remove information about the private attribute while maintaining data utility. Overall, a modest level of negative conditioning, e.g., $w_S = 0.03$, strikes a favorable balance between utility and privacy on the MotionSense dataset.

I. Quantifying Disentanglement Capability of Contrastive Classifier-Free Guidance

We corroborate the effectiveness of CCFG in disentangling the public attribute and other attributes on the 5-attribute AudioMNIST dataset, with the spoken digit serving as the public attribute. The contrastive encoder ϕ was trained for 30 epochs, and MI between its learned latent representations (\mathbf{z}_U) and every attribute was estimated using the Mutual Information Neural Estimator (MINE) [41]. Note that CCFG does not require knowledge of the private attribute to perform

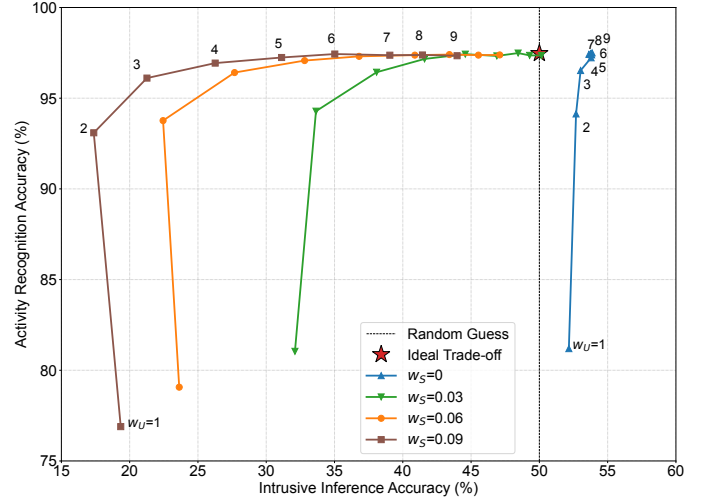


Fig. 4. CLOAK's privacy-utility trade-off on MotionSense

disentanglement. Figure 5 shows the change in MI over 30 training epochs, where the line with markers and color band represent mean \pm std across 5 runs.

It can be seen that the MI between \mathbf{z}_U and the public attribute (digit) consistently increased throughout the training of the contrastive encoder ϕ , demonstrating CCFG's effectiveness in maintaining utility. Conversely, the MI with other attributes, namely gender, age, accent, and user ID, peaked around the 5th epoch, because when ϕ is first trained to include information on the public attribute, information on other attributes will also be included due to the entanglement. However, after the 5th epoch, the MI between \mathbf{z}_U and other attributes significantly decreased by an average of 67.37% (gender), 61.62% (age), 57.22% (accent), and 57.23% (user ID), without affecting the MI with the public attribute. This confirms that CCFG can disentangle information about the public attribute from all other attributes, thereby improving the privacy-utility trade-

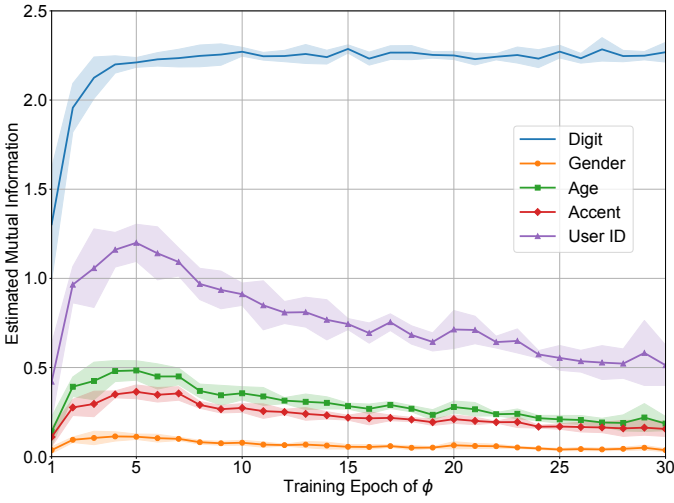


Fig. 5. Estimated mutual information between contrastively learned \mathbf{z}_U and attributes on AudioMNIST

off.

J. Defending Against Re-identification Attacks

In this section, we consider a more powerful adversary that has access to both the obfuscated data and the corresponding ground-truth private attribute labels. This adversary performs a re-identification attack [4] by training a model M_R on the obfuscated data to predict the private attribute class. We use the MotionSense dataset as a case study and reuse the CLOAK model presented in Section V-F to perform data obfuscation. The obfuscated data samples \mathbf{x}' and their associated private attribute labels (gender) are divided into training and test sets following the same ratio as in Section V-A2. M_R adopts the same model architecture as the intrusive inference model M_S and is trained using the same pipeline and hyperparameters. We repeat the experiments for five trials and report the average results. We find that M_R attains an average accuracy of 54.00% in predicting the true gender from the obfuscated data, corresponding to a privacy loss of 4.00%, with a standard deviation of 1.26%. Moreover, we observe that the model has difficulty converging during training, achieving an average training accuracy of only $54.42\% \pm 1.49\%$. This result indicates that even when an adversary has full access to a sufficient amount of obfuscated data and the true private attribute labels, training a CNN model to recover the private attribute from obfuscated data remains very challenging, as evident from the near-random-guessing performance. This demonstrates that data obfuscated by CLOAK contains minimal information about the private attributes.

K. Conditioning Multiple Public/Private Attributes

CLOAK can be extended by conditioning on multiple public attributes to support more downstream applications or conditioning on multiple private attributes to obscure more than one private attribute.

To support K public attributes U_1, \dots, U_K , for each public attribute U_i , we utilize a dedicated contrastive encoder

TABLE IV
RESULTS OF CONDITIONING MULTIPLE PUBLIC ATTRIBUTES ON MOBIACT DATASET, PUBLIC ATTRIBUTES: ACTIVITY (ACT.) AND WEIGHT, PRIVATE ATTRIBUTE: GENDER.

Metric	Accuracy (%)		L_S (%)
Attribute	U_1 -Act. (\uparrow)	U_2 -Weight (\uparrow)	S -Gender (\downarrow)
Raw Data	98.87 ± 0.00	91.74 ± 0.00	47.51 ± 0.00
CLOAK	94.47 ± 1.01	80.18 ± 2.16	8.82 ± 0.89

TABLE V
RESULTS OF CONDITIONING MULTIPLE PRIVATE ATTRIBUTES ON MOBIACT DATASET, PUBLIC ATTRIBUTE: ACTIVITY (ACT.), PRIVATE ATTRIBUTES: GENDER AND WEIGHT.

Metric	Accuracy (%)			Privacy Loss L_S (%)
Attribute	U -Act. (\uparrow)	S_1 -Gender (\downarrow)	S_2 -Weight (\downarrow)	L_S (%)
Raw Data	98.87 ± 0.00	47.51 ± 0.00	58.41 ± 0.00	
CLOAK	98.25 ± 0.12	0.79 ± 1.90	0.39 ± 0.45	

ϕ_i trained to extract disentangled latent representations \mathbf{z}_{U_i} . We condition the diffusion-based obfuscation model with the concatenated latent representations of the K public attributes: $\mathbf{z}_C = \mathbf{z}_{U_1} \oplus \dots \oplus \mathbf{z}_{U_K}$, then replace \mathbf{z}_U with \mathbf{z}_C in Eq. (7) to train a diffusion model conditioned on the K public attributes.

To protect K private attributes S_1, \dots, S_K , we train K auxiliary classifiers η_1, \dots, η_K to predict the corresponding private attribute from the raw sensor data. CLOAK aims to compute $p_{\theta, \phi, \eta_1, \dots, \eta_K}(\mathbf{z}_t | U, \bar{S}_1, \dots, \bar{S}_K)$. Assuming that the K private attributes are conditionally independent, we follow the derivation of (8) (9) (10) to obtain the updated noise predictor with K private attributes:

$$\bar{\epsilon}_\theta(\mathbf{z}_t, t, U, S_1, \dots, S_K) = (1 + w_U)\epsilon_\theta(\mathbf{z}_t, t, U) - w_U\epsilon_\theta(\mathbf{z}_t, t) + \sum_{i=1}^K w_{S_i} \sqrt{1 - \bar{a}_t} \nabla_{\mathbf{z}_t} \log p_\eta(S_i | U, \mathbf{z}_t), \quad (13)$$

where w_{S_i} is the hyperparameter that controls the strength of negative conditioning for the private attribute S_i . This enables guiding the data obfuscation model during sampling using compositional negated classifier guidance.

1) *Experiment results:* We evaluate the effectiveness of conditioning multiple public or private attributes on MobiAct. For conditioning multiple public attributes, we consider activity and weight as the public attributes, and gender as the private attribute. For conditioning multiple private attributes, we consider activity to be the public attribute and both gender and weight group as private attributes. The remaining experimental details are the same as we described in the main paper. We report mean \pm std computed over 5 runs.

We present the results of conditioning CLOAK on multiple public attributes in Table IV. For the public attributes, activity, and weight, CLOAK achieves average desired inference accuracy of 94.47% and 80.18%, a decline of 4.40% and 11.56% compared to the raw data, respectively. The average privacy loss of the gender attribute is 8.82%. When CLOAK is conditioned on two public attributes, the entanglement

between public and private attributes becomes stronger, yielding a worse privacy-utility trade-off compared to when it is conditioned on a single public attribute. Although a larger w_S can further reduce the privacy loss, we notice that the data utility could deteriorate to a greater extent. Nevertheless, CLOAK still reduces the privacy loss by 38.69% compared to raw data while offering reasonable data utility.

Next, we condition CLOAK to protect multiple private attributes at the same time, and show the results in Table V. CLOAK can effectively reduce the privacy loss on both private attributes, gender, and weight, to the random guessing level. In this case, extending the protection to the weight attribute results in a negligible compromise on data utility. Compared to the results in Table II, the average activity recognition accuracy remains at the same level, while the privacy loss for weight is reduced by 8.19% on average. This demonstrates that CLOAK can be easily extended to protect multiple private attributes.

L. Evaluation of Computational Overhead

We compare the computational overhead of CLOAK with PrivDiffuser, considering model size, number of parameters, and sampling time per data segment. In addition, we deploy CLOAK on an Nvidia Jetson to evaluate the real-world obfuscation latency on edge IoT platforms.

We denote the surrogate utility model used in PrivDiffuser and the contrastive encoder ϕ used in CLOAK as Aux-U, and the auxiliary privacy models used for negative conditioning in both obfuscation models as Aux-S. CLOAK’s VAE learns latent representations of size 60, and its encoder is not involved in the sampling process. In Table VI, we report the overhead of both obfuscation models measured on MotionSense. The model size is calculated in FP32 precision. We sample obfuscated data using 50 timesteps per batch, for a total of 50 batches, with a batch size of 128. We report the average GPU execution time for obfuscating one data segment on an NVIDIA RTX 2080 Ti.

The Aux-Us used in both obfuscation models share the same architecture, resulting in the same negligible sampling time (0.03 ms). The Aux-S models used for classifier guidance are also computationally efficient to run and exhibit negligible time overhead. However, the size of Aux-S in CLOAK is less than 1% of the size of Aux-S in PrivDiffuser, as CLOAK operates in a latent space that is much smaller than the input space and uses only FC layers rather than the CNN architecture as used in PrivDiffuser. The size of UNet in CLOAK is $\sim 46\%$ smaller than the size of UNet in PrivDiffuser, thanks to the benefit of operating in the latent space. Moreover, CLOAK uses 1D convolutional kernels in the UNet to accommodate the 1D latent representations, further reducing the overhead of 2D convolutional operations. As a result, the sampling time of CLOAK’s UNet is only 28.85 ms, a speed up of $4.72\times$ compared to PrivDiffuser. This indicates that utilizing the LDM architecture for the UNet yields the greatest improvement in the sampling overhead. Despite the additional model size from the variational decoder, CLOAK achieves a $1.51\times$ reduction in the total model size and the number of parameters. Since

TABLE VI
OVERHEAD COMPARISON BETWEEN PRIVDIFFUSER (P) AND CLOAK (C)
FOR GENDER OBFUSCATION ON MOTIONSENSE.

Model	Size (MB)	# Params	Samp. Time (ms)
P: UNet	271.05	71.05M	136.38
P: Aux-U	130.41	34.19M	0.03
P: Aux-S	130.53	34.22M	0.00
P: Total	531.99	139.46M	136.41
C: UNet	146.54	38.41M	28.85
C: Decoder	28.14	7.38M	0.02
C: Aux-U	130.41	34.19M	0.03
C: Aux-S	0.89	0.23M	0.00
C: Total	305.98	80.21M	28.90

PrivDiffuser can perform real-time obfuscation on modern edge platforms [5], CLOAK, which is more efficient, can be deployed on a wider range of resource-constrained mobile IoT devices.

Lastly, we evaluate CLOAK’s obfuscation latency on edge IoT platforms by deploying it on an Nvidia Jetson AGX Xavier with 16 GB of memory. We consider the gender-obfuscation task on MotionSense as a case study, demonstrating that CLOAK is suitable for deployment on resource-constrained devices. We perform data obfuscation in batches of 128 data segments, while keeping the remaining experimental setups unchanged. We directly run the model trained on a server in FP32 precision without applying any specialized optimization for the Jetson platform. We measure the data-obfuscation time over 20 batches and compute the average latency. On average, obfuscating one batch of data segments takes 26.05 seconds, corresponding to an obfuscation latency of 203.5 ms per data segment. If motion sensors have a sampling rate of 50 Hz and the sliding window used for data segmentation has a stride length of 10 samples, an obfuscation latency of approximately 200 ms would enable real-time obfuscation—closely matching CLOAK’s measured latency per data segment. Real-world deployment could further leverage frameworks such as TensorRT and techniques like quantization and lower precision (e.g., FP16) to reduce memory footprint and sampling time.

VI. CONCLUSION

We introduce CLOAK, a lightweight sensor data obfuscation model based on latent diffusion models. We propose a contrastive learning-based guidance technique, dubbed CCFG, for conditioning the LDM on public attributes; paired with a negated classifier guidance for conditioning on the private attributes, CLOAK offers flexible, fine-grained control over the privacy-utility trade-off without requiring model retraining. We demonstrate that contrastive learning enables effective information disentanglement in CLOAK, allowing it to outperform baselines that rely on mutual information-based regularization or adversarial training. Specifically, extensive evaluations on four time-series datasets and one image dataset demonstrate that CLOAK consistently achieves state-of-the-art privacy-utility trade-offs, improving desired inference accuracy on the public attribute by up to 7.21%, and reducing intrusive

inference accuracy on the private attribute by up to 5.76%. Moreover, we show that CLOAK can be easily extended to protect multiple public or private attributes. Further, we deploy CLOAK on an Nvidia Jetson platform to corroborate that it can perform real-time obfuscation on edge IoT platforms. In future work, we aim to explore the scalability of CLOAK by conditioning more public or private attributes and investigate if the distribution of the contrastive encoder’s training data could impact CLOAK’s generalizability.

REFERENCES

- [1] M. Malekzadeh *et al.*, “Mobile sensor data anonymization,” in *Proceedings of the International Conference on Internet-of-Things Design and Implementation*, 2019, pp. 49–58.
- [2] B. Wüggenmann, V. Rublack, M. Andrejczuk, J. Mattern, and F. Kerschbaum, “Dp-vae: Human-readable text anonymization for online reviews with differentially private variational autoencoders,” in *Proceedings of the ACM Web Conference 2022*, 2022, pp. 721–731.
- [3] H. Choi, S. S. Woo, and H. Kim, “Blind-touch: Homomorphic encryption-based distributed neural network inference for privacy-preserving fingerprint authentication,” in *Proceedings of the AAAI conference on artificial intelligence*, vol. 38, no. 20, 2024, pp. 21976–21985.
- [4] O. Hajihassnai *et al.*, “ObscureNet: Learning attribute-invariant latent representation for anonymizing sensor data,” in *Proceedings of the International Conference on Internet-of-Things Design and Implementation*, 2021, pp. 40–52.
- [5] X. Yang and O. Ardakanian, “Privdiffuser: Privacy-guided diffusion model for data obfuscation in sensor networks,” *Proceedings on Privacy Enhancing Technologies*, vol. 2025, no. 4, pp. 40–55, 2025.
- [6] S. Liu *et al.*, “Privacy adversarial network: representation learning for mobile data privacy,” *Proceedings of the ACM on Interactive, Mobile, Wearable and Ubiquitous Technologies*, vol. 3, no. 4, pp. 1–18, 2019.
- [7] A. Li *et al.*, “DeepObfuscator: Obfuscating intermediate representations with privacy-preserving adversarial learning on smartphones,” in *Proceedings of the International Conference on Internet-of-Things Design and Implementation*, 2021, pp. 28–39.
- [8] A. Li *et al.*, “TIPRDC: Task-independent privacy-respecting data crowdsourcing framework for deep learning with anonymized intermediate representations,” in *Proceedings of the 26th ACM SIGKDD International Conference on Knowledge Discovery & Data Mining*, 2020, pp. 824–832.
- [9] N. Raval *et al.*, “Olympus: Sensor privacy through utility aware obfuscation.” *Proceedings on Privacy Enhancing Technologies*, vol. 2019, no. 1, pp. 5–25, 2019.
- [10] Y. Chen *et al.*, “MaSS: Multi-attribute selective suppression for utility-preserving data transformation from an information-theoretic perspective,” in *Proceedings of the 41st International Conference on Machine Learning*, 2024, pp. 6519–6538.
- [11] M. Bertran, N. Martinez, A. Papadaki, Q. Qiu, M. Rodrigues, G. Reeves, and G. Sapiro, “Adversarially learned representations for information obfuscation and inference,” in *International Conference on Machine Learning*. PMLR, 2019, pp. 614–623.
- [12] Z. Wu, H. Wang, Z. Wang, H. Jin, and Z. Wang, “Privacy-preserving deep action recognition: An adversarial learning framework and a new dataset,” *IEEE Transactions on Pattern Analysis and Machine Intelligence*, vol. 44, no. 4, pp. 2126–2139, 2020.
- [13] I. R. Dave, C. Chen, and M. Shah, “Spect: Self-supervised privacy preservation for action recognition,” in *Proceedings of the IEEE/CVF Conference on Computer Vision and Pattern Recognition*, 2022, pp. 20 164–20 173.
- [14] Y. Deng *et al.*, “Disentangled and controllable face image generation via 3d imitative-contrastive learning,” in *Proceedings of the IEEE/CVF conference on computer vision and pattern recognition*, 2020, pp. 5154–5163.
- [15] X. Ren, T. Yang, Y. Wang, and W. Zeng, “Learning disentangled representation by exploiting pretrained generative models: A contrastive learning view,” in *International Conference on Learning Representations*, 2022. [Online]. Available: <https://openreview.net/pdf?id=j63FSNcO5a>
- [16] A. v. d. Oord, Y. Li, and O. Vinyals, “Representation learning with contrastive predictive coding,” *arXiv preprint arXiv:1807.03748*, 2018.
- [17] Q. Wu, Y. Liu, H. Zhao, A. Kale, T. Bui, T. Yu, Z. Lin, Y. Zhang, and S. Chang, “Uncovering the disentanglement capability in text-to-image diffusion models,” in *Proceedings of the IEEE/CVF conference on computer vision and pattern recognition*, 2023, pp. 1900–1910.
- [18] T. Yang, Y. Wang, Y. Lu, and N. Zheng, “Disdiff: Unsupervised disentanglement of diffusion probabilistic models,” *Advances in Neural Information Processing Systems*, vol. 36, pp. 69 130–69 156, 2023.
- [19] Y. Dalva and P. Yanardag, “Noiseclr: A contrastive learning approach for unsupervised discovery of interpretable directions in diffusion models,” in *Proceedings of the IEEE/CVF Conference on Computer Vision and Pattern Recognition*, 2024, pp. 24 209–24 218.
- [20] T. Qi *et al.*, “Deadiff: An efficient stylization diffusion model with disentangled representations,” in *Proceedings of the IEEE/CVF Conference on Computer Vision and Pattern Recognition*, 2024, pp. 8693–8702.
- [21] R. Rombach *et al.*, “High-resolution image synthesis with latent diffusion models,” in *Proceedings of the IEEE/CVF conference on computer vision and pattern recognition*, 2022, pp. 10 684–10 695.
- [22] A. Radford *et al.*, “Learning transferable visual models from natural language supervision,” in *International Conference on Machine Learning*. PMLR, 2021, pp. 8748–8763.
- [23] Y. Leng, Q. Huang, Z. Wang, Y. Liu, and H. Zhang, “Diffusegai: controllable and high-fidelity image manipulation from disentangled representation,” in *Proceedings of the 5th ACM International Conference on Multimedia in Asia*, 2023, pp. 1–7.
- [24] T. Yang, C. Lan, Y. Lu, and N. Zheng, “Diffusion model with cross attention as an inductive bias for disentanglement,” in *The Thirty-eighth Annual Conference on Neural Information Processing Systems*, 2024.
- [25] A. Wu and W.-S. Zheng, “Factorized diffusion autoencoder for unsupervised disentangled representation learning,” in *Proceedings of the AAAI Conference on Artificial Intelligence*, vol. 38, no. 6, 2024, pp. 5930–5939.
- [26] M. Armandpour *et al.*, “Re-imagine the negative prompt algorithm: Transform 2D diffusion into 3D, alleviate Janus problem and beyond,” *arXiv preprint arXiv:2304.04968*, 2023.
- [27] P. Dhariwal and A. Nichol, “Diffusion models beat GANs on image synthesis,” *Advances in Neural Information Processing Systems*, vol. 34, pp. 8780–8794, 2021.
- [28] J. Ho, A. Jain, and P. Abbeel, “Denoising diffusion probabilistic models,” *Advances in Neural Information Processing Systems*, vol. 33, pp. 6840–6851, 2020.
- [29] D. P. Kingma, M. Welling *et al.*, “Auto-encoding variational bayes,” 2013.
- [30] J. Ho and T. Salimans, “Classifier-free diffusion guidance,” *arXiv preprint arXiv:2207.12598*, 2022.
- [31] P. Dong *et al.*, “Towards test-time refusals via concept negation,” *Advances in Neural Information Processing Systems*, vol. 36, 2024.
- [32] N. Liu *et al.*, “Compositional visual generation with composable diffusion models,” in *European Conference on Computer Vision*. Springer, 2022, pp. 423–439.
- [33] A. Bansal *et al.*, “Universal guidance for diffusion models,” in *Proceedings of the IEEE/CVF Conference on Computer Vision and Pattern Recognition*, 2023, pp. 843–852.
- [34] C. Chatzaki *et al.*, “Human daily activity and fall recognition using a smartphone’s acceleration sensor,” in *International Conference on Information and Communication Technologies for Ageing Well and e-Health*. Springer, 2016, pp. 100–118.
- [35] A. Bahaa’A *et al.*, “A dataset for wi-fi-based human activity recognition in line-of-sight and non-line-of-sight indoor environments,” *Data in Brief*, vol. 33, p. 106534, 2020.
- [36] S. Becker, J. Vielhaben, M. Ackermann, K.-R. Müller, S. Lapuschkin, and W. Samek, “Audiomnist: Exploring explainable artificial intelligence for audio analysis on a simple benchmark,” *Journal of the Franklin Institute*, vol. 361, no. 1, pp. 418–428, 2024.
- [37] W.-N. Hsu, B. Bolte, Y.-H. H. Tsai, K. Lakhotia, R. Salakhutdinov, and A. Mohamed, “Hubert: Self-supervised speech representation learning by masked prediction of hidden units,” *IEEE/ACM transactions on audio, speech, and language processing*, vol. 29, pp. 3451–3460, 2021.
- [38] E. Eidinger, R. Enbar, and T. Hassner, “Age and gender estimation of unfiltered faces,” *IEEE Transactions on information forensics and security*, vol. 9, no. 12, pp. 2170–2179, 2014.
- [39] O. Ronneberger, P. Fischer, and T. Brox, “U-net: Convolutional networks for biomedical image segmentation,” in *Proceedings of the 18th Interna-*

tional Conference on Medical Image Computing and Computer-Assisted Intervention. Springer, 2015, pp. 234–241.

- [40] J. Song, C. Meng, and S. Ermon, “Denoising diffusion implicit models,” *arXiv preprint arXiv:2010.02502*, 2020.
- [41] M. I. Belghazi *et al.*, “Mutual information neural estimation,” in *International conference on machine learning*. PMLR, 2018, pp. 531–540.